Micromechanical imaging of dentin with Brillouin microscopy

Tijana Lainović, Jérémie Margueritat, Quentin Martinet, Xavier Dagany, Larisa Blažić, Dejan Pantelić, Mihailo D Rabasović, Aleksandar J Krmpot, Thomas Dehoux

Brillouin microscopy for nondestructive mechanical imaging of dentin

Tijana Lainović,[1] Jérémie Margueritat,[2] Quentin Martinet,[2] Xavier Dagany,[2] Larisa Blažić,[1,3] Dejan Pantelić,[4] Mihailo D. Rabasović,[4] Aleksandar J. Krmpot,[4] Thomas Dehoux[2*]

[1] Faculty of Medicine, School of Dentistry, University of Novi Sad, Hajduk Veljkova 3, 21000 Novi Sad, Serbia

[2] Univ Lyon, Univ Claude Bernard Lyon 1, CNRS, Institut Lumière Matière, F-69622, Villeurbanne, France

[3]Dental Clinic of Vojvodina, Hajduk Veljkova 12, 21000 Novi Sad, Serbia

[4] Institute of Physics Belgrade, University of Belgrade, Pregrevica 118, 11080 Belgrade, Serbia

*email: thomas.dehoux@univ-lyon1.fr

ABSTRACT

The physical structure of teeth can be altered by diet, age or diseases such as caries or sclerosis. It is of utmost importance to characterize the mechanical properties to predict and understand tooth decay, to design restorative dental procedure, and to investigate the tribological behavior of teeth. Yet, existing imaging techniques are unable to reveal the micromechanics of the tooth, in particular at tissue interfaces. Here we developed a microscope based on Brillouin light scattering (BLS) to probe mechanical changes in tooth tissues. BLS is an inelastic process that uses the scattering of light by acoustic waves in the GHz range. Our microscope thus reveals the mechanical properties at a sub-micrometer scale without contact to the sample. BLS signals show significant differences between healthy tissues and pathological lesions, and allow delineating precisely destructed dentin. We also show maps of the sagittal and transversal planes of healthy tubular dentin that reveal its anisotropic microstructure with a 1 μm resolution, several orders of magnitude below previous reports. Our observations indicate that the collagen-based matrix of dentine is the main load bearing structure, which can be thought of as a fiber-reinforced composite. In the vicinity of polymeric tooth-filling materials, we observed fingering of the adhesive complex into the opened tubules of healthy dentine. The ability to probe the quality of this interfacial layer could lead to innovative designs of biomaterials used for dental restorations in contemporary adhesive dentistry, and would have direct repercussions on the decision-making during clinical work.

INTRODUCTION

Human dentin is an organized, hard, mineralized tissue of the tooth, composed of 70 wt% calcified tissue (hydroxyapatite), 20 wt% organic phase (mostly composed of collagen type I as well as other fibrils), and 10 wt% water [1]. It is perfused with microtubules that allow sensory communication to the underlying pulp and nerves.[2] This fiber-composite-like structure yields an anisotropic distribution of mechanical properties that support masticatory stress concentrated in the surrounding enamel.[3] Tooth mechanical strength can be altered by diet, age or diseases such as caries or sclerosis.[44] It is of utmost importance to characterize mechanical properties during tooth life in order to predict and understand tooth decay, to design restorative dental procedure, and to investigate the tribological behavior of teeth.

Most of the characterization means are inherited from material science, and involve destructive testing such as indentation or fatigue tests. [3, 17] Due to the variety of techniques and the complexity of the dentin microstructure, there is a lack of quantified consensus on the mechanical properties of dentin.[38] Moreover, such approaches are clearly difficult to put into practice *in vivo*. In the clinic, dentinal pathological changes can be detected by visuo-tactile and radiographic methods to guide clinicians in establishing a relevant diagnostic, and in proposing an adequate therapy.[4] However, such approaches cannot give precise information on the microstructure, cannot delineate precisely caries margins, [5] and are highly depend on the clinician [6].

Acoustic techniques have long been used to probe the mechanics of dentin, initially analyzing the reflection or transmission of ultrasonic pulses emitted from a piezoelectric transducer in the MHz range. [39] Later implementations in tooth tissues in various healthy and pathological states used resonant ultrasonic spectroscopy, [38] acoustic microscopy,[7, 8, 9] surface waves [10] or laser ultrasonics. [11], [12] However, these techniques are limited to the MHz range, i.e. a ~ 100 μm resolution, unable to reveal the micromechanics of the tooth, in particular at tissue interfaces.

State-of-the-art microscopies, such as multiphotonic or non-linear technologies, [41] can offer optical resolution but cannot provide any information on the mechanics of the sample. Laser spectroscopies have recently rose to prominence, offering quantitative imaging of the chemical structure of tooth tissues and restorative materials. [13, 14, 15, 16] In this paper we propose a new approach to probe acoustic waves in the GHz range by laser spectroscopy, thus offering quantitative microscopy with a contrast based on the mechanical properties of tooth tissues.

We developed a microscope based on Brillouin light scattering (BLS) to probe mechanical changes in tooth tissues. BLS is an inelastic process similar to Raman scattering. Raman-based techniques rely on the scattering of light by optical phonons, and operate at THz frequencies. They provide information on the molecular structure of the sample. By contrast, Brillouin scattering uses the scattering of light by acoustic phonons.[18] Since acoustic phonons have lower energies than optical phonons, Brillouin scattering produces frequency shifts in the GHz range that reveal the mechanical properties of the sample. Developed in the 60's for solid-state physics, BLS has only recently emerged as a key technology in life sciences due to its ability to produce non-contact, label-free microscopic images of the mechanical properties of cells and tissues. [19] It has notably been applied for the analysis of biological fibers, connective tissues and muscles [17, 20, 21], eye tissues [22, 23], bone [24, 26] or tumors.[35]

We prepared thick slices of teeth extracted in accordance with the ethical requirements for ex-vivo studies. We obtained maps of Brillouin frequency shift and linewidth that can be interpreted as maps of sound velocity and viscosity. Our results show significant changes between healthy tissues and pathological lesions. Such results allow delineating precisely destructed dentin, paving the way to minimally invasive strategies. We also show maps of the sagittal and transversal planes of healthy tubular dentin that reveal its anisotropic microstructure with a 1 μm resolution, several orders of magnitude below previous reports.[38] Our observations indicate that the collagen-based matrix of dentine is the main load bearing structure, which can thought of as fiber-reinforced composite. In the vicinity of polymeric tooth-filling materials, we observed fingering of the adhesive complex into the opened tubules of healthy dentine. We confirmed our observations with two-photon excitation fluorescence (2PEF) and second harmonic generation (SHG) microscopies that reveal teeth

microstructure due to two-photon excited autofluorescence and collagen-specific second order nonlinear optical susceptibility [27]. The ability to probe the quality of this interfacial layer could lead to innovative designs of biomaterials used for dental restorations in contemporary adhesive dentistry, and would have direct repercussions on the decision-making during clinical work.

MATERIALS AND METHODS.

Sample preparation and staining.

Teeth were collected at Faculty of Medicine, School of Dentistry, at the Department of Oral Surgery of Dental Clinic of Vojvodina, Serbia. They were extracted for medical reasons and, after the patient's consent, approved to be used for research purposes according to the protocol of Ethical board of Dental Clinic of Vojvodina, Serbia. All types of permanent teeth were analyzed, including incisors, canines, premolars and molars. The teeth were classified in the following groups: healthy teeth with intact hard tissues (two subgroups – teeth cut perpendicularly to their longitudinal axis, teeth cut longitudinally), teeth with caries lesions in dentin [score 5 on the International Caries Detection and Assessment System (ICDAS) scale; distinct cavity with visible dentin], restored teeth with composite resin.

Teeth restored with composite used for the imaging of the dentin-adhesive interface were prepared according to the standard dental adhesive placement procedure, after the etching procedure by using 37% orto-phosporic acid for 15 seconds, rinsing it, and placing a single bond universal adhesive (3M Deutschland GmbH, LOT 663414), before restoration with the Filtek Ultimate Body composite. For 2PEF imaging of dentin-adhesive interface, a water solution containing 0.5% eosin-Y was added in small quantities into the adhesive in order to distinguish the adhesive from the surrounding dentinal tissue.

Teeth were sectioned into ~0.5 mm thick slices along the horizontal and longitudinal axes, by a water-cooled, low speed diamond saw using a hard tissues microtome. Samples were wet-polished with abrasive sandpaper sheets of silicone-carbide of increasing grit numbers (400-2000). This was followed by polishing with a diamond paste on a soft fabric, in order to eliminate the surface corrugations. The smear layer produced by polishing was removed by 10% polyacrylic acid used for 5 seconds, after which the samples were rinsed, slightly dry-aired and disinfected in 0,5% chloramine solution and preserved in plastic bags until examined.

Nonlinear laser scanning microscopy

Teeth specimens were observed by a nonlinear optical microscopy setup at the Institute of Physics in Belgrade. The homemade nonlinear laser-scanning microscope used in this study has been described in detail elsewhere.[42, 43] Briefly, a Ti:Sapphire femtosecond laser (Coherent, Mira 900-F) tunable in 700-1000nm range, and a Yb:KGW (Time-Bandwidth Products AG, Yb GLX) femtosecond laser at 1040nm were used as a laser light sources. The samples were imaged using Carl Zeiss, EC Plan-NEOFLUAR, 40×1.3 oil immersion objective or Plan-APOCHROMAT 20x/0.8 air objective for laser focusing and collection of the signal. A visible interference filter (415 nm–685 nm) positioned in front of the detector is used to remove scattered laser light in fluorescence images. Thus, the whole visible range has been detected in two-photon fluorescence images. The tooth auto-fluorescence was excited by the Ti:Sapphire laser at 730nm. The Eosin-Y fluorescence was excited by the Ti:Sapphire laser at

820nm. Narrowband interference filters (10 nm FWHM) were used for second harmonic generation imaging. The SHG filter central wavelength was 520nm (FB520-10, Thorlabs) for the Yb:KGW laser. The SHG filter central wavelength was 420nm (FB420-10, Thorlabs) for Ti:Sapphire laser when tuned at 840nm. The SHG excitation wavelength and filter were selected so that fluorescence leakage to SHG channel is minimal.

Brillouin spectroscopy

BLS uses the scattering of light by phonons. Thermal phonons (incoherent vibrations) produce a broad peak at low frequencies due to Rayleigh scattering, while acoustic phonons (coherent vibration) with wavenumbers that fulfill the Bragg condition produce well-defined peaks (**Figure 1**). Using a monochromatic light beam of wavelength λ in a normal incidence backscattering geometry, forward propagating phonons produce a positive shift at a frequency $f = 2nV/\lambda$ (anti-Stokes peak), where V is the sound velocity and n is the refractive index, typically in the GHz range (backward propagating phonons creates a negative Stokes peak at $-f$).

Assuming that the sample is homogeneous over the scattering volume, the BLS spectra can be interpreted as the response of a damped harmonic oscillator with frequency position f and full width at half maximum Γ. In this approximation, the storage modulus is $' = \rho(f\lambda/2n)^2$, where ρ is the mass density. The linewidth Γ is ascribed to the loss modulus $M'' = \rho\Gamma f(\lambda/2n)^2$. In other words, the frequency shift and linewidth can be interpreted as the sound velocity (or stiffness) and viscosity of the sample. Note that at the high magnifications we use, Γ can artificially increase due to scattering.

Brillouin microscope

The Brillouin spectrometer is based on a tandem Fabry-Pérot interferometer (JRS Scientific Instruments). [35] In order to reduce phototoxicity, we used a $\lambda = 647.1$ nm continuous-wave laser as a light source (instead of classical designs based on a frequency-doubled YAG laser at 532~nm) which gives a $\frac{\lambda}{2n} \approx 200$ nm acoustic resolution, where $n = 1.6$ is the typical refractive index of dentin. The spectrometer offers a 40 GHz free spectral range sampled with a 30~MHz sampling rate. Appropriate signal analysis allows reaching a 6 MHz accuracy at a -10 dB noise level. It is equipped with two sets of mirrors with a 95% reflectivity, and an avalanche photodiode (Count® Blue, Laser Components) with a dark count lower than 10 counts/sec (typically 2counts/sec) and a quantum efficiency of 65% at this wavelength. The spectrometer is coupled with an inverted life science microscope (Eclipse Ti-U, Nikon) equipped with a micro-positioning stage (Mad City Labs). The collimated linearly-polarized laser light is focused onto the sample using a $100\times$ objective lens (NA 0.9), offering a ~1 μm resolution. The typical power used at the focus was 5~mW, resulting in a power density over the scattering volume a hundred times smaller than that previously reported in tissues and cells, again to ensure low phototoxicity. The backscattered light is collected by the same objective lens and is collected outside the microscope using a telescope. A particular attention has been paid to respect the f-number (f/18) of the spectrometer in order to maximize photon collection on the photodiode. Spectra were acquired by averaging typically over ~100 acquisitions.

Data analysis

Raw spectra sampled at 30 MHz are recorded by the proprietary software of the spectrometer (Ghost software, Table Stable Ltd., Switzerland). When only one peak is observed on each side of the Rayleigh line (see **Fig. 1b** for instance), we fit separately the anti-Stokes and Stokes peaks to a Lorentzian function using Matlab and extract amplitude A, frequency shift f and linewidth Γ. Values for each peak are then averaged. When two closely-spaced peaks are observed, we window sequentially around each peak and fit them individually with a single Lorentzian function. This procedure might underestimate slightly the true spacing between the two peaks, but it reducing the error of the fit and hence allows automating the fitting procedure to analyze large images.

The data collected on the different groups of samples were statistically analyzed using Matlab software. The level of significance (p-value) was evaluated according to an unpaired two-tailed t-test.

RESULTS.

Mechanical signature of caries lesions

Brillouin spectra were recorded for healthy tissues ($n = 34$ in 5 different teeth) and caries lesions ($n = 39$ in 5 different teeth). Care was taken to focus the laser beam in the regions that didn't show tubules. For illustration, we plot in **Fig. 1** a typical spectrum. **Figure 1a** shows that the raw spectrum is dominated by Rayleigh scattering (grey box). **Figure 1b** shows a zoom-in on the Stokes (negative frequencies) and anti-Stokes (positive frequencies) peaks for the healthy tissue and caries lesion. We fit these peaks with Lorentzian functions (dashed lines) to extract the frequency shift f and linewidth Γ (**Methods**). The distributions of frequency and linewidth values are plotted in **Figs. 2a** and **2b**, respectively. Note that the spreading of the data is larger in the case of caries because BLS features depend on the position within the highly heterogeneous lesion, as discussed below. Frequency shift is clearly different between healthy and diseased conditions. We don't however observe any significant variation in the linewidth. This observation suggest that BLS features could be used to delineate lesions.

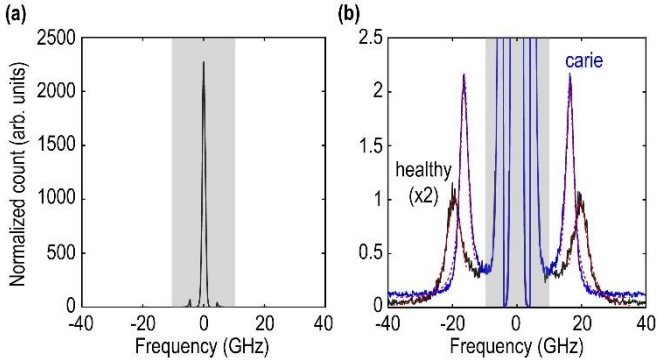

Figure 1: typical spectrum. *(a) Raw spectrum where the contribution of Rayleigh scattering is indicated by the grey box. (b) Zoom-in on the Stokes (negative frequencies) and anti-Stokes (positive frequencies) peaks for a healthy tissue (black, intensity multiplied by 2 for clarity) and a caries lesion (blue line). Fits by Lorentzian functions are superimposed (red dashed lines).*

To investigate this, we scanned the laser along a line across the frontier between healthy tissue and a caries lesion. **Figure 3** shows the frequency shift f and linewidth Γ measured from the healthy region (left) to the core of the lesion (right). We see that, as already observed in **Fig. 2b**, Γ does not vary. On the other hand, f decreases slowly, making the precise delineation difficult. As a reference, we indicate the median (red dashed line) and the 25th and 75th percentiles (grey box) measured in **Fig. 2a**. The upward arrow indicates where f falls below the 25th percentile. This criterion might be used to define the limit of the healthy tissue. In this example, f decrease almost linearly by ~ 0.01 GHz/µm within the lesion. Given the spreading of the data for healthy dentin measured in **Fig. 2a**, ~ 0.2 GHz between the mean and the 25th percentile, such decrease would lead to a 20 µm precision in the identification of the lesion margins.

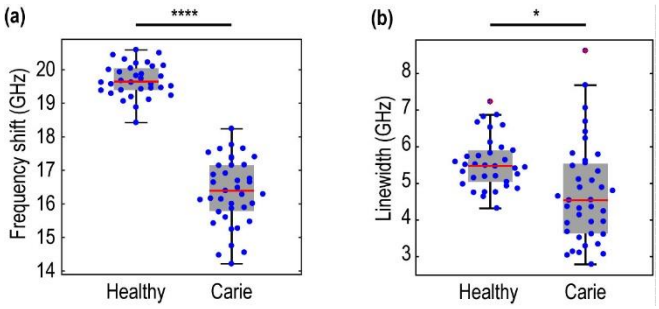

Figure 2: Comparison between healthy tissues (n=34) and caries lesions (n=39). *Distributions of (a) frequency shift and (b) linewidth (****p<0.0001, *p<0.05, unpaired two-tailed t-test). The bottom and top edges of each grey box indicate the 25th and 75th percentiles, respectively. The red central line indicates the median. The whiskers extend to the most extreme data points not considering outliers ('+' symbol).*

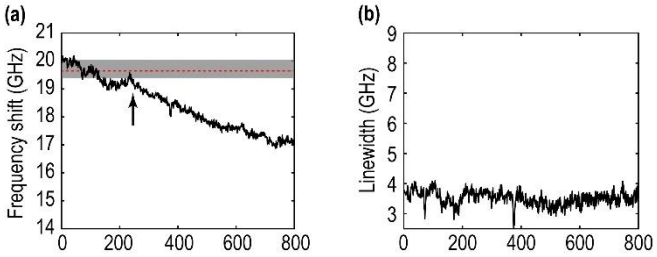

Figure 3: scan across a caries lesion. *(a) frequency shift and (b) linewidth. The grey box and red dashed line indicate the 25th and 75th percentiles and median identified in Fig. 2a. Upward arrow indicates the position where the frequency shift falls below the 25th percentile.*

Mechanical anisotropy of the dentin

Healthy dentin is composed of a mineralized matrix perfused by microtubes called tubules. This structure leads to an anisotropic distribution of mechanical properties, largely documented in the literature on a macroscale.[38] To investigate the anisotropy of the healthy tubular dentin on a microscopic scale, healthy teeth were cut longitudinally or transversally (**Methods**). The microstructure of the healthy dentin in the sagittal and transversal planes is well revealed by the combination of 2PEF image obtained with the Ti:Sapphire tuned at 730 nm and SHG image obtained with the Ti:Sapphire tuned at 840 nm (**Figures 4 and 5**). The typical tubular structure of dentin appears clearly on the 2PEF image. Collagen type I, as a triple-helical molecule, the organic component on

which the dentin is mostly built, is aligned in a non-centrosymmetric manner, and is responsible for the contrast in the SHG images. The SHG images of dentin thus reveal the intertubular dentin, which is less mineralized than the peritubular dentin.[28]

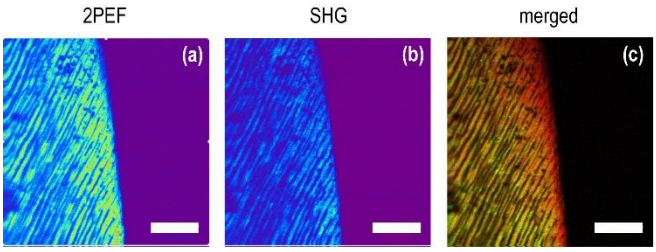

Figure 4: 2PEF and SHG images of healthy dentin in the sagittal plane. *(a) 2PEF image reveal the tubular structure of dentin, (b) SHG reveals the presence of collagen type I, (c) merged. Scale bars: 20 µm.*

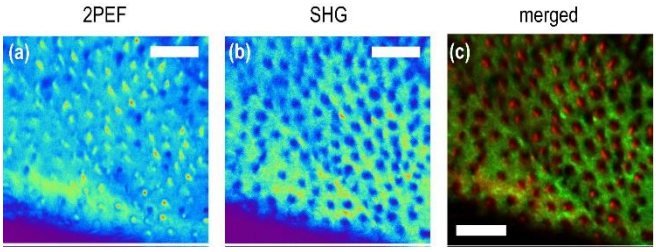

Figure 5: 2PEF and SHG images of healthy dentin in the transversal plane. *(a) 2PEF image reveal the tubular structure of dentin, (b) SHG reveals the presence of collagen type I, (c) merged. Scale bars: 20 µm.*

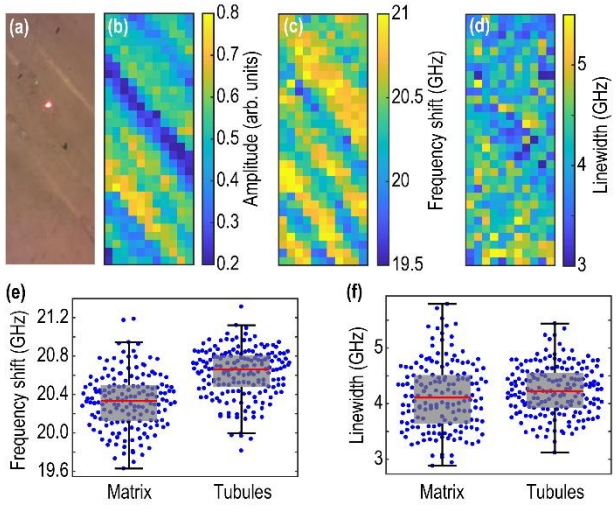

Figure 6: images of healthy dentin in the sagittal plane. *(a) optical image, (b) amplitude of the Brillouin peaks, (c) frequency shift and (d) linewidth. Panels (e) and (f) show the distribution of f and Γ-values measured in panels (c) and (d), respectively. The tubules are identified in panel (b) by amplitude values lower than 50% of the maximum amplitude, and the matrix correspond to remaining pixels.*

The exposed surfaces in the sagittal and transversal planes were mapped with BLS. The laser was scanned in a raster pattern with a 1 μm resolution and spectra recorded at each pixel. Resulting images obtained in the sagittal (along the tubules) and transversal planes (perpendicular to the tubules) of the

tooth are shown in **Figs. 6** and **7**, respectively. In the sagittal plane, the tubules are clearly visible on the optical image (**Fig. 6a**), and they are characterized by a lower amplitude (**Fig. 6b**) and a lower f (**Fig. 6c**). We define an amplitude threshold $A_{th} = 0.5A_m$, where A_m is the maximum amplitude, that separates the tubules from the surrounding matrix. Pixels in the f and Γ images that correspond to an amplitude $A < A_{th}$ are ascribed to the tubules, and the remaining pixels to the matrix. The distribution of pixels for f and Γ are shown in **Figs. 6e** and **6f**. While the linewidth doesn't allow distinguishing the two components (as observed on **Fig. 6d**), f-values are slightly higher for the tubules.

In the transverse plane, the tubules appear as disks on the optical image (**Fig. 7a**). They are also clearly visible on the BLS images, characterized here too by a low amplitude (**Fig. 7b**). In this case however, the low amplitude of the Brillouin peaks does not allow to identify f or Γ-values in the tubular regions, and only the matrix appears in the f and Γ images, **Figs. 7d** and **7f**. This is because the tubules cause a depression in the transverse plane that defocuses the laser beam. Considering pixels where $A < A_{th}$ thus only reveals the distributions of values for the matrix, plotted in **Figs. 7c** and **7e**, respectively. The f and Γ values differ slightly in the sagittal and transverse planes, suggesting that the matrix itself is anisotropic.

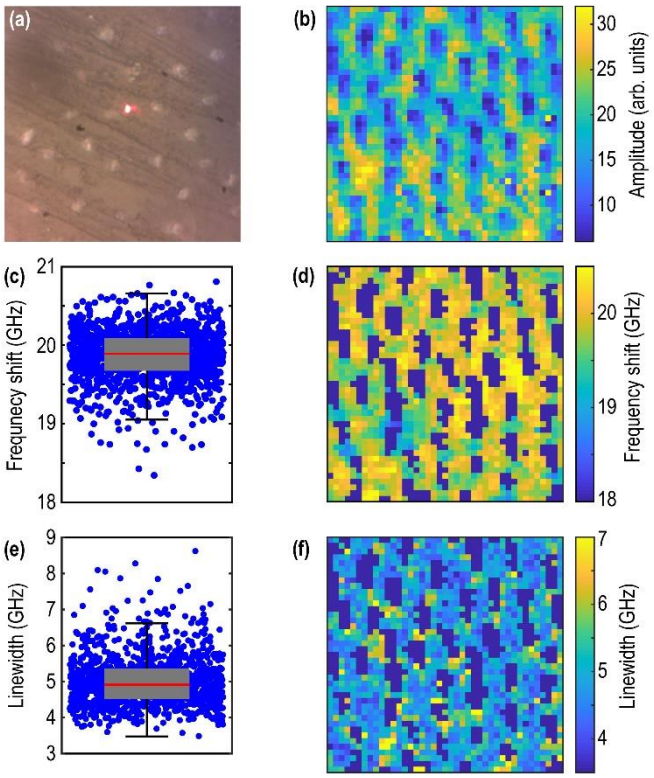

Figure 7: images of healthy dentin in the transversal plane. *(a) optical image, (b) amplitude of the Brillouin peaks, (d) frequency shift and (f) linewidth. Panels (c) and (e) show the distribution of f and Γ-values measured in panels (d) and (f), respectively.*

Characterization of the dentin-resin interface

In this section we examine the adhesive interface between healthy dentin and tooth-filling resin. **Figure 8a** shows a typical sample with adhesive interface indicated by the arrow. Merged 2PEF image obtained with the Ti:Sapphire tuned at 820 nm and SHG image obtained with the Yb:KGW (**Figure 8b)** reveals the typical structure of the interface between dentin (SHG, blue pseudocolor) and adhesive (labelled by eosin in 2PEF, red pseudocolor). This image reveals that the low-viscous monomer adhesive fingers in-between the exposed dentinal collagen fibers of intertubular dentin, or in the tubules themselves, forming the so-called hybrid layer. Extensions of monomer entering a few individual dentinal tubules, i.e. resin tags, are also observable (a typical one is pointed at by a white arrow).

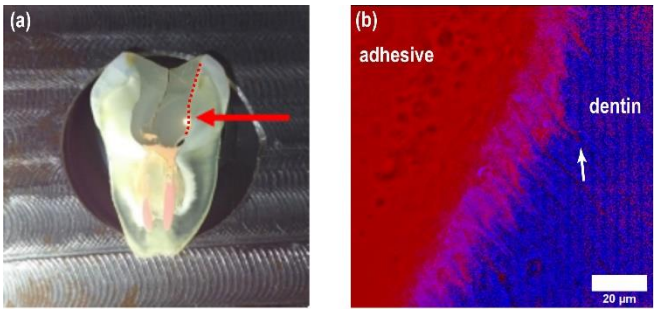

Figure 8: structure of a typical dentin adhesive interface. *(a) photograph of dentin-resin adhesive interface shown by dashed line and the arrow. (b) Merged 2PEF and SHG images of a dentin-adhesive interface. 2PEF micrograph reveals the adhesive colored by eosin Y (red pseudocolor) and SHG micrograph reveals dentin (blue pseudocolor). Arrow points to a typical resin tag. Scale bar: 20 µm.*

We probed the interface between healthy dentin and resin with BLS. **Figure 9a** shows a typical spectrum where we recognize the signature of healthy dentin at around 20 GHz (blue area). In addition, we also observe a second peak at around 13 GHz (pink area), revealing the presence of the adhesive. This result demonstrates that BLS is able to detect the presence of the two components mixed in the hybrid layer. To investigate this, we recorded BLS images in a typical hybrid layer. The frequency shift (**Fig. 9b**) and linewidth (**Fig. 9c**) both allow to observe the adhesive, hybrid layer and dentin. This clearly highlights the ability of BLS to quantify adhesive interfaces, and to reveal the fingering of the adhesive in the hybrid layer. Such results should pave the way for novel strategies for tooth repair.

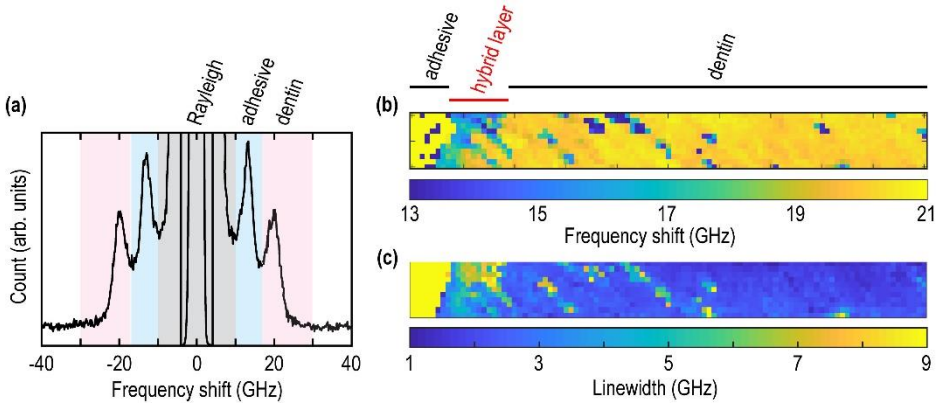

Figure 9: imaging the hybrid layer. *(a) typical spectrum at the dentin-adhesive interface. The peaks arising from dentin and adhesive are shown in blue and pink, respectively. (a) Frequency shift and (b) linewidth maps of the hybrid layer.*

DISCUSSION.

We have demonstrated the potential of BLS to examine non-destructively and with high resolution the mechanical properties of different healthy, diseased or restored dental tissues. The BLS maps in the sagittal and transverse planes clearly reveal the tubular structure of dentin. Our results showed $f_s \sim 20.4$ GHz in the sagittal plane, and $f_t \sim 19.8$ GHz in the transverse plane for the matrix alone. These values correspond to sound velocities $V_s = \frac{f\lambda}{2n_s} \approx 4100$ m/s and $V_t = \frac{f\lambda}{2n_t} \approx 4300$ m/s, assuming refractive indices $n_s = 1.6$ and $n_t = 1.5$ in the sagittal and transverse plane, respectively.[37] From these values we can estimate the storage moduli $M_s' = \rho V_s^2 \sim 36$ GPa and $M_t' = \rho V_t^2 \sim 38$ GPa, where $\rho \sim 2100$ kg/m^3 is the mass density (**Methods**).[36] This matches very well with previous results, ~37–39 GPa, obtained by ultrasonic interferometry.[40]

Our data shows an anisotropy of 6% and stiffer values in the transverse plane. Since the tubules are aligned in the softer sagittal plane, this observation demonstrates that the tubules do not contribute to mechanical strength of dentine. Instead, the mineralized collagen fibrils, aligned in the stiffer transverse plane, act as a load bearing structure, as suggested previously.[38] This means that the anisotropy of dentine originates from the anisotropy of the matrix itself, and that its structure could be thought as a fiber-reinforced composite material in the transverse plane.

The difference between frequencies of healthy dentin and those of caries lesions is very clear ($p < 0.0001$). The transition from healthy dentin to caries allows delineation with a 20 µm precision for the samples we probed. The linewidth $\Gamma = 2\pi\eta(2n/\lambda)^2$ is constant across this region, meaning that both n and kinematic viscosity η are constant. The change in f can thus be ascribed to a reduction in the stiffness of the tooth in the lesion. This observation demonstrates the high specificity of BLS, and the ability to produce quantitative indicators of tooth decay. In contemporary clinical practice, the visuo-tactile method is the dominant approach to caries delineation, and is obviously less resolved than BLS and operator-dependent. In order to avoid inter-examiner variations, visual examination can be aided by dyes, light-fluorescence based methods, or fiber-optic transillumination. In this context, BLS has a unique potential to provide quantitative information at a microscale, in a label-free, non-invasive, non-ionizing manner. Further comparison with histological sections of lesions with different scores should reveal the sensitivity of BLS, and grant new minimally invasive strategies in dentistry. As has been done for cancer therapy [35], ophthalmology [30] or bone,[25] BLS could be used as a platform for early diagnosis of tooth decay, micrometric precise caries detection during clinical work, but also for the monitoring of efficacy of the therapeutic techniques. [31, 34]

BLS images of the hybrid layer bring new information on the spatial distribution of mechanical properties in the adhesive junction. In future, BLS could be used to test the adhesion strength of different types of adhesives under preclinical investigation, or the weakening of the hybrid layer by enzyme-caused degradation of collagen or adhesive, mineral-depleted dentin[31, 32] or caries lesion [33]. Moreover, the hybrid layer is subjected to multiaxial stresses during functional use, and it has

been predicted that stress concentration in the underlying hard dental tissues depends on the stiffness of this interface [29]. In future, BLS could also help studying the impact of wear on this interface at a microscale. Beyond dentistry, BLS could also provide new tools to investigate the link between microwear, stiffness and diet, offering important information in paleobiology.

ACKNOWLEDGEMENTS.

The work was partly supported by the COST Action CA16124 "Brillouin Light Scattering Microspectroscopy for Biological and Biomedical Research and Applications", the Agence Nationale de la Recherche (Grant No. ANR-17-CE11-0010-01), and the Ministry of Education, Science and Technological Development of Serbia (projects TR35020, III 45016, ON 171038). The authors thank Tatjana Maravić and the team of professor Bojan Petrović (Faculty of Medicine, School of Dentistry, University of Novi Sad) for their support in samples preparation.

REFERENCES.

[1] M. Goldberg, A. B. Kulkarni, M. Young, and A. Boskey, "Dentin: structure, composition and mineralization," Front. Biosci. (Elite Ed), vol. 3, p. 711, 2011.

[2] S. R. Stock, A. C. Deymier-Black, A. Veis, A. Telser, E. Lux, and Z. Cai, "Bovine and equine peritubular and intertubular dentin," Acta Biomater, vol. 10, p. 3969, 2014.

[3] J. H. Kinney, M. Balooch, S. J. Marshall, G. W. Marshall JR, and T. P. Weihs, "Hardness and Young's modulus of human peritubular and intertubular dentine," Arch. Oral Biol., vol. 41, no. I, pp. 9–13, 1996.

[4] S. K. Makhijaa, M. E. Robinson, J. D. Bader, D. A. Shugars, M. S. Litaker, H. R. Im, D. B. Rindal, D. J. Pihlstrom, C. Meyerowitz, V. V Gordan, M. H. Buckberg, and G. H. Gilbert, "Dentists' decision strategies for suspicious occlusal caries lesions in a National Dental PBRN study," J. Dent., vol. 69, p. 83, 2018.

[5] F. Schwendicke, S. Paris, and Y.-K. Tu, "Effects of using different criteria for caries removal: A systematic review and network meta-analysis," J. Dent., vol. 43, no. 1, pp. 1–15, 2015.

[6] G. J. Joves, G. Inoue, A. Sadr, T. Nikaido, and J. Tagami, "Nanoindentation hardness of intertubular dentin in sound , demineralized and natural caries-affected dentin," J. Mech. Behav. Biomed. Mater., vol. 32, pp. 39–45, 2014.

[7] R. Maev, L. Denisova, E. Maeva, and D. AA, "New data on histology and physico-mechanical properties of human tooth tissue obtained with acoustic microscopy.," Ultrasound Med Biol, vol. 28, pp. 131–136, 2002.

[8] K. Raum, K. Kempf, H. J. Hein, J. Schubert, and P. Maurerb, "Preservation of microelastic properties of dentin and tooth enamel in vitro—A scanning acoustic microscopy study," Dent. Mater., vol. 2 3, pp. 1221–1228, 2007.

[9] A. Shelke, M. Blume, M. Mularczyk, C. Landes, R. Sader, and J. Bereiter-Hahn, "Visualisation of localized elastic properties in human toth and jawbone as revealed by scanning acoustic microscopy," Ultrasound Med. Biol, vol. 39, no. 5, pp. 853–859, 2013.

[10] S. Toda, T. Fujita, H. Arakawa, and K. Toda, “Nondestructive testing in human teeth using a leaky Lamb wave device,” Ultrasonics, vol. 44, pp. e1151–e1155, 2006.

[11] K. Sun, L. Yuan, Z. Shen, Q. Zhu, J. Lu, and X. Ni, “Experimental and numerical studies for nondestructive evaluation of human enamel using laser ultrasonic technique,” Appl. Opt., vol. 52, no. 28, pp. 6896–6905, 2013.

[12] H.-C. Wang, S. Fleming, Y.-C. Lee, M. Swain, S. Law, and J. Xue, “Laser ultrasonic evaluation of human dental enamel during remineralization treatment,” Biomed. Opt. Express, vol. 2, no. 2, pp. 345–355, 2011.

[13] H. Salehi, E. Terrer, I. Panayotov, B. Levallois, B. Jacquot, H. Tassery and F. Cuisinier, "Functional mapping of human sound and carious enamel and dentin with Raman spectroscopy", J. Biophotonics 6, 765-774 (2013).

[14] R. Ramakrishnaiah, G. ur Rehman, S. Basavarajappa, A. A. Al Khuraif, B. H. Durgesh, A. S. Khan, and I. ur Rehman, “Applications of Raman Spectroscopy in Dentistry: Analysis of Tooth Structure,” Appl Spectrosc Rev, vol. 50, no. 4, pp. 332–350, 2015.

[15] C. de C. A. Lopes, P. H. J. O. Limirio, V. R. Novais, and P. Dechichi, “Fourier transform infrared spectroscopy (FTIR) application chemical characterization of enamel, dentin and bone,” Appl. Spectrosc. Rev., vol. 53, no. 9, pp. 747–769, 2018.

[16] Z. A. Steelman, D. S. Ho, K. K. Chu and A. Wax, "Light-scattering methods for tissue diagnosis", Optica 6, 479-489 (2019).

[17] R. Harley, D. James, A. Miller, and J. W. White, “Phonons and the elastic moduli of collagen and muscle,” Nature, vol. 267, pp. 285–287, 1977.

[18] L. Brillouin, “Diffusion de la lumière et des rayonnés X par un corps transparent homogène; influence de l’agitation thermique,” Ann. Phys., vol. 17, pp. 88–122, 1922.

[19] F. Palombo and D. Fioretto, "Brillouin Light Scattering: Applications in Biomedical Sciences", Chem. Rev. 119, 7833-7847 (2019).

[20] J. Randall, J. M. Vaughan, and S. Cusak, “Brillouin scattering in systems of biological significance,” Philos. Trans. R. Soc. A, vol. 293, pp. 341–348, 1979.

[21] F. Palombo, C. P. Winlove, R. S. Edginton, E. Green, N. Stone, S. Caponi, M. Madami, and D. Fioretto, “Biomechanics of fibrous proteins of the extracellular matrix studied by Brillouin scattering,” J. R. Soc. Interface, vol. 11, p. 20140739, 2014.

[22] J. M. Vaughan and J. T. Randall, “Brillouin scattering, density and elastic properties of the lens and cornea of the eye,” Nature, vol. 284, no. 5755, pp. 489–491, 1980.

[23] G. Scarcelli and S. H. Yun, “Confocal Brillouin microscopy for three-dimensional mechanical imaging,” Nat. Photonics, vol. 2, no. 1, p. 39, 2008.

[24] S. Lees, N. J. Tao, and S. M. Lindsay, “Studies of compact hard tissues and collagen by means of brillouin light scattering,” Connect. Tissue Res., vol. 24, no. 3–4, pp. 187–205, 1990.

[25] R. Tsubota, K. Fukui, and M. Matsukawa, “Local ultrasonic wave velocities in trabeculae measured by micro-Brillouin scattering,” J. Acoust. Soc. Am., vol. 2, pp. EL109-EL114, 135AD.

[26] V. Mathieu, K. Fukui, M. Matsukawa, M. Kawabe, R. Vayron, E. Soffer, F. Anagnostou, and G. Haiat, “Micro-Brillouin Scattering Measurements in Mature and Newly Formed Bone

Tissue Surrounding an Implant," J. Biomech. Eng., vol. 133, no. February, pp. 021006-1-021006-6, 2011.

[27] M. Oheim, D. Michael, M. Geisbauer, M. Dorte, and R. Chow, "Principles of two-photon excitation fluorescence microscopy and other nonlinear imaging approaches," Adv. Drug Deliv. Rev., vol. 58, pp. 788–808, 2006.

[28] R. Elbaum, E. Tal, A. I. Perets, D. Oron, D. Ziskind, Y. Silberberg, and H. D. Wagner, "Dentin micro-architecture using harmonic generation microscopy," J. Dent., vol. 35, no. 2, pp. 150–155, 2007.

[29] A. Misra, V. Singh, and R. Parthasarathy, Material-tissue interfacial phenomena: Challenges in mathematical modeling. Elsevier Ltd, 2016.

[30] S. H. Yun and D. Chernyak, "Brillouin microscopy: assessing ocular tissue biomechanics," Curr. Opin. Ophthalmol., vol. 29, no. 4, pp. 299–305, 2018.

[31] S. Sauro, V. P. Feitosa, T. F. Watson, and D. H. Pashley, "Therapeutic bonding approaches to remineralize dentin-bonded interfaces," Dent. Mater., vol. 32, no. Supplement 1, pp. e3–e4, 2016.

[32] M. Hashimoto, H. Ohno, H. Sano, M. Kaga, and H. Oguchi, "In vitro degradation of resin–dentin bonds analyzed by microtensile bond test, scanning and transmission electron microscopy," Biomaterials, vol. 24, pp. 3795–3803, 2003.

[33] M. Oliveir, F. Chasqueira, S. Arantes-Oliveira, and S. Pessanha, "The use of micro-Raman spectroscopy for the analysis of caries-aff ected dentin adhesive interfaces." p. In Press.

[34] S. Sauro, R. Osorio, T. F. Watson, and M. Toledano, "Influence of phosphoproteins ' biomimetic analogs on remineralization of mineral-depleted resin – dentin interfaces created with ion-releasing resin-based systems," Dent. Mater., vol. 31, no. 7, pp. 759–777, 2015.

[35] J. Margueritat, A. Virgone-Carlotta, S. Monnier, H. Delanoë-Ayari, H. C. Mertani, A. Berthelot, Q. Martinet, X. Dagany, C. Rivière, J.-P. Rieu, and T. Dehoux, "High-frequency mechanical properties of tumors measured by Brillouin light scattering", Phys Rev. Lett. 122, 018101 (2019).

[36] Regine Gradl, Irene Zanette, Maite Ruiz-Yaniz, Martin Dierolf, Alexander Rack, Paul Zaslansky, and Franz Pfeiffer, " Mass Density Measurement of Mineralized Tissue with Grating-Based X-Ray Phase Tomography", PLoS ONE 11, e0167797 (2016).

[37] I. Hariri, A. Sadr, Y. Shimada, J. Tagami, and Y. Sumi, "Effects of structural orientation of enamel and dentine on light attenuation and local refractive index: An optical coherence tomography study", J. Dentistry 40, 2012

[38] J. H. Kinney, S. J. Marshall and G. W. Marshall, "The mechanical properties of human dentin: a critical review and re-evaluation of the dental litterature", Crit. Rev. Oral. Biol. Med. 14, 13-29 (2003)

[39] G. Kossoff and C. J. Sharpe, "Examination of the contents of the pulp cavity in teeth", Ultrasonics 4, 77-83 (1966).

[40] S. Lees and F. R. Rollins, "Anisotropy in hard dental tissues", J. Biomech. 5, 557-566 (1972).

[41] T. Cloitre, I. V. Panayotov, H. Tassery, C. Gergely, B. Levallois and F. J. Cuisinier, "Multiphoton imaging of the dentine-enamel junction", J. Biophotonics 6, 330-337 (2013).

[42] M. Rabasović, D. Pantelić, B. Jelenković, S. Ćurčić, M. Rabasović, M. Vrbica, et al., "Nonlinear microscopy of chitin and chitinous structures: a case study of two cave-dwelling insects", J. Biomed. Opt. 20, 016010 (2015).

[43] K. Bukara, S. Z. Jovanić, I. T. Drvenica, A. Stančić, V. Ilić, M. D. Rabasović, D. V. Pantelić, B. M. Jelenković, B. Bugarski and A. J. Krmpot, "Mapping of hemoglobin in erythrocytes and erythrocyte ghosts using two photon excitation fluorescence microscopy" J. Biomed. Opt. 22, 026003 (2017)

[44] D. Zaytsev, S. Grigoriev and P. Panfilov, "Deformation behavior of root dentin under Sjogren's syndrome", Mat. Lett. 65, 2435-2438 (2011).